Broadband infrared meanderline reflective quarter-wave plate

Samuel L. Wadsworth,* and Glenn D. Boreman

University of Central Florida, CREOL – The College of Optics and Photonics, 4000 Central Florida Blvd., Orlando, FL, 32816, USA

**swadswor@creol.ucf.edu*

Abstract: We present a novel reflective quarter-wave plate comprised of subwavelength meanderline elements. The device is operational over the long-wave infrared (LWIR) spectrum, with significant spectral and angular bandwidths. Power reflection is approximately 70% over the majority of the LWIR. Efficient conversion from a 45° linear polarization state into circular polarization is demonstrated from finite-element electromagnetic simulations and from broadband polarimetric measurements.

OCIS codes: (260.3060) Infrared; (230.5440) Polarization-selective devices; (050.6624) Subwavelength structures.

References and links

1. E. H. Korte, B. Jordanov, D. Kolev, and D. Tsankov, "Total reflection prisms as achromatic IR retarders," Appl. Spectrosc. **42**(8), 1394–1400 (1988).
2. R. M. A. Azzam and H. K. Khanfar, "In-line broadband 270 ° (3λ/4) chevron four-reflection wave retarders," Appl. Opt. **47**(27), 4878–4883 (2008).
3. E. Cojocaru, T. Julea, and F. Nichitiu, "Infrared thin-film totally reflecting quarter-wave retarders," Appl. Opt. **30**(28), 4124–4125 (1991).
4. R. M. A. Azzam and C. L. Spinu, "Achromatic angle-insensitive infrared quarter-wave retarder based on total internal reflection at the Si-SiO_2 interface," J. Opt. Soc. Am. A **21**(10), 2019–2022 (2004).
5. J. Liu and R. M. A. Azzam, "Infrared quarter-wave reflection retarders designed with high-spatial-frequency dielectric surface-relief gratings on a gold substrate at oblique incidence," Appl. Opt. **35**(28), 5557–5562 (1996).
6. V. N. Okorkov, V. Y. Panchenko, B. V. Russkikh, V. N. Seminogov, V. I. Sokolov, and V. P. Yakunin, "Phase retarder for transformation of polarization of high-power infrared laser beams based on resonant excitation of surface electromagnetic waves on metallic diffraction gratings," Opt. Eng. **33**(10), 3145–3155 (1994).
7. Y. Pang and R. Gordon, "Metal nano-grid reflective wave plate," Opt. Express **17**(4), 2871–2879 (2009).
8. V. G. Niziev and A. V. Nesterov, "Influence of beam polarization on laser cutting efficiency," J. Phys. D Appl. Phys. **32**(13), 1455–1461 (1999).
9. K. C. Hwang, "Optimization of broadband twist reflector for Ku-band application," Electron. Lett. **44**(3), 210–211 (2008).
10. K. Y. Han and B. A. Lail, "Genetically-engineered meanderline twist reflector," Antennas and Propagation Society International Symposium, AP-S (2008).
11. J. Hanfling, G. Jerinic, and L. Lewis, "Twist reflector design using *E*-type and *H*-type modes," IEEE Trans. Antenn. Propag. **29**(4), 622–629 (1981).
12. B. A. Munk, *Frequency-Selective Surfaces: Theory and Design* (Wiley, 2000).
13. S. L. Wadsworth and G. D. Boreman, "Analysis of throughput for multilayer infrared meanderline waveplates," Opt. Express **18**(13), 13345–13360 (2010).
14. J. S. Tharp, B. A. Lail, B. A. Munk, and G. D. Boreman, "Design and demonstration of an infrared meanderline phase retarder," IEEE Trans. Antenn. Propag. **55**(11), 2983–2988 (2007).
15. C. Terret, J. R. Levrel, and K. Mahdjoubi, "Susceptance computation of a meander-line polarizer layer," IEEE Trans. Antenn. Propag. **32**(9), 1007–1011 (1984).
16. R.-S. Chu and K.-M. Lee, "Analytical method of a multilayered meander-line polarizer plate with normal and oblique plane-wave incidence," IEEE Trans. Antenn. Propag. **35**(6), 652–661 (1987).
17. J.-C. Zhang, Y.-Z. Yin, and J.-P. Ma, "Multifunctional meander line polarizer," Prog. Electromagn. Res. Lett. **6**, 55–60 (2009).
18. P. A. Rizzi, *Microwave Engineering: Passive Circuits* (Prentice-Hall, 1988).
19. C. S. R. Kaipa, A. B. Yakovlev, F. Medina, F. Mesa, C. A. M. Butler, and A. P. Hibbins, "Circuit modeling of the transmissivity of stacked two-dimensional metallic meshes," Opt. Express **18**(13), 13309–13320 (2010).
20. B. J. Rubin and B. Singh, "Study of meander line delay in circuit boards," IEEE Trans. Microw. Theory Tech. **48**(9), 1452–1460 (2000).
21. R.T. Remski, "Analysis of photonic bandgap surfaces using Ansoft HFSS," Microwave J. **43**, 190–198 (2000).

#146273 - $15.00 USD Received 19 Apr 2011; revised 6 May 2011; accepted 6 May 2011; published 13 May 2011

22. N. R. Labadie and S. K. Sharma, "A novel compact volumetric metamaterial structure with asymmetric transmission and polarization conversion," Metamaterials (Amst.) **4**(1), 44–57 (2010).
23. W. R. Folks, J. C. Ginn, D. J. Shelton, J. S. Tharp, and G. D. Boreman, "Spectroscopic ellipsometry of materials for infrared micro-device fabrication," Phys. Status Solidi C **5**(5), 1113–1116 (2008).
24. D. Goldstein, *Polarized Light* (Marcel Dekker, 2003).
25. J. E. Raynolds, B. A. Munk, J. B. Pryor, and R. J. Marhefka, "Ohmic loss in frequency-selective surfaces," J. Appl. Phys. **93**(9), 5346–5358 (2003).
26. J. S. Tharp, D. J. Shelton, S. L. Wadsworth, and G. D. Boreman, "Electron-beam lithography of multiple-layer submicrometer periodic arrays on a barium fluoride substrate," J. Vac. Sci. Technol. B **26**(5), 1821–1823 (2008).

1. Introduction

Reflective quarter-wave plates (QWPs) for the infrared (IR) have utilized several different technologies to achieve circularly polarized (CP) light upon reflection [1–7]. For instance, reflective prisms [1,2] with or without thin-film interference layers [3,4] have been demonstrated to provide a $\pi/2$ phase shift between orthogonal field components over a broad spectrum of IR wavelengths. Additionally, microstructured surfaces have been shown to produce QWP behavior over a narrow band typically centered on 10.6 μm while simultaneously achieving high reflectivity [5–7]. Their intended application is industrial CO_2-laser welding and machining, since the focused spot from CP radiation has excellent uniformity [5,6,8]. Although the aforementioned devices are well-suited for their intended applications, they do have a few drawbacks. In particular, the reflective QWP prisms are quite bulky and expensive, and the reflective microstructured phase retarders are typically optimized only for a narrow spectrum around the design wavelength [5,6]. Ideally, a component would combine a low-cost compact planar structure with broadband performance. Subwavelength elements as broadband reflective phase retarders have been previously demonstrated in the microwave regime as a polarization twister, which rotates the plane of polarization by 90° upon imparting a π phase retardance between orthogonal field amplitudes [9–11]. One such design of a twist reflector incorporated the versatile meanderline frequency-selective-surface (FSS) unit cell element [9,10,12], which has recently been shown to provide achromatic transmissive QWP behavior in the LWIR [13,14]. We adapt this LWIR meanderline concept for use as a broadband reflective QWP.

2. Design of a broadband reflective meanderline QWP

The meanderline FSS structure can be described by an equivalent-circuit model, which has been used previously for accurate predictions of meanderline performance in both the microwave [15–17] and IR [13]. As shown in Fig. 1, a meanderline structure is fabricated on a dielectric layer, so the meanderline-dielectric surface collectively represents a single planar discontinuity that can be modeled as a single shunt admittance element [13,16–19], added to the equivalent circuit of the planar dielectric and groundplane. The dielectric layer is represented by finite-length transmission lines with wave impedances characteristic of the associated optical materials [13,16,18,19]. The short-circuit termination represents the reflective groundplane of the meanderline QWP structure, consistent with previous reflective designs [9–11].

#146273 - $15.00 USD Received 19 Apr 2011; revised 6 May 2011; accepted 6 May 2011; published 13 May 2011

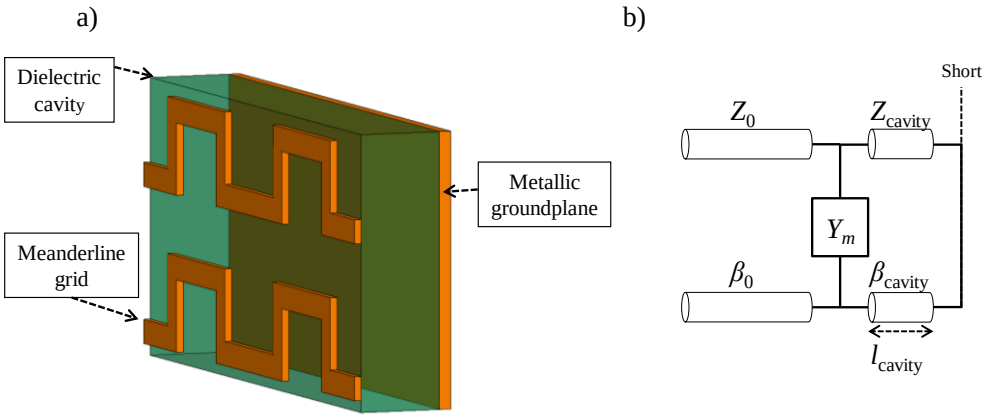

Fig. 1. Diagram of a) meanderline geometry patterned on a dielectric cavity above groundplane, and b) equivalent circuit model of multilayer dielectric system with meanderline discontinuity as the shunt admittance Y_m.

The interaction between incident IR radiation and the meanderline can be visualized in terms of a complex-valued wave impedance that depends upon the incident state of polarization and the geometrical configuration of the patterned conductors [12,13,16,19]. This description is prevalent throughout all literature relating to meanderline retarders and FSS in general, since the transverse-electric (TE) and transverse-magnetic (TM) components of the field have been shown to experience separate equivalent impedances upon interaction with a meanderline structure [12,13,15,16]. For instance, the TE component passes between the horizontally-aligned meanderline structure, which imparts a capacitive impedance. Likewise, the TM component induces a large current flow through the meanderline conductors, yielding an inductive impedance. These opposing impedances provide a phase retardance equal to the difference in phase between the TE and TM modes [12–17]. For reflective meanderline QWPs, the phase retardance would accumulate over multiple successive transmissions through the meanderline structure, both forwards and backwards, since the fields reflect off of the metallic groundplane and induce resonant-cavity modes inside the dielectric standoff layer [16,18]. This is seen schematically in Fig. 2, which shows the equivalent circuit of the overall QWP. An alternate description of the structure as a delay circuit is given in [20], where the TM mode is scattered with a phase delay corresponding to the travel time of the induced current along the meanderline.

#146273 - $15.00 USD Received 19 Apr 2011; revised 6 May 2011; accepted 6 May 2011; published 13 May 2011

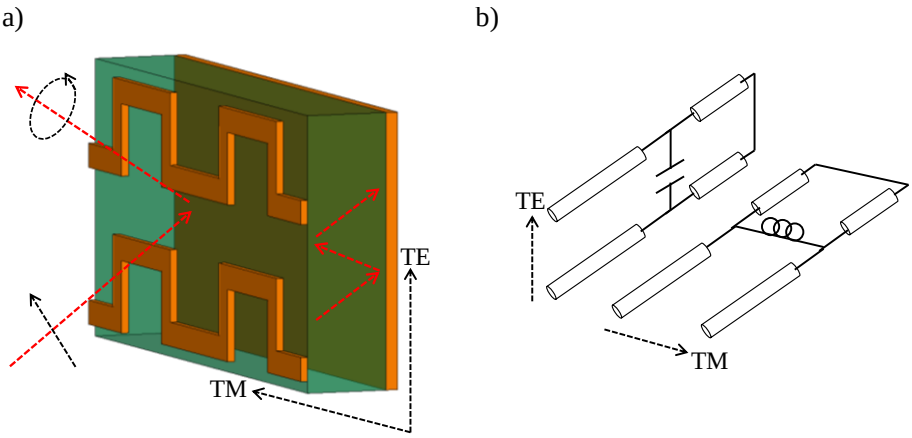

Fig. 2. Depiction of a) meanderline geometry with incident linearly-polarized wave, reflected CP field, and multiple reflections inside dielectric cavity. Part b) represents the equivalent circuit elements of the meanderline grid that are encountered by the respective TE and TM modes of the incident wave.

The design of the structure emphasizes optimization of design parameters to obtain an achromatic phase retardance and a high reflectivity over the LWIR band of interest. The design of a broadband reflective meanderline QWP was carried out within the ANSYS High Frequency Structure Simulator (HFSS), a finite-element-method (FEM) electromagnetic full-wave solver that uses Floquet ports to model planar periodic arrays [21,22]. A Newtonian search algorithm internal to the HFSS program was used to refine the geometrical parameters, which are shown in Fig. 3.

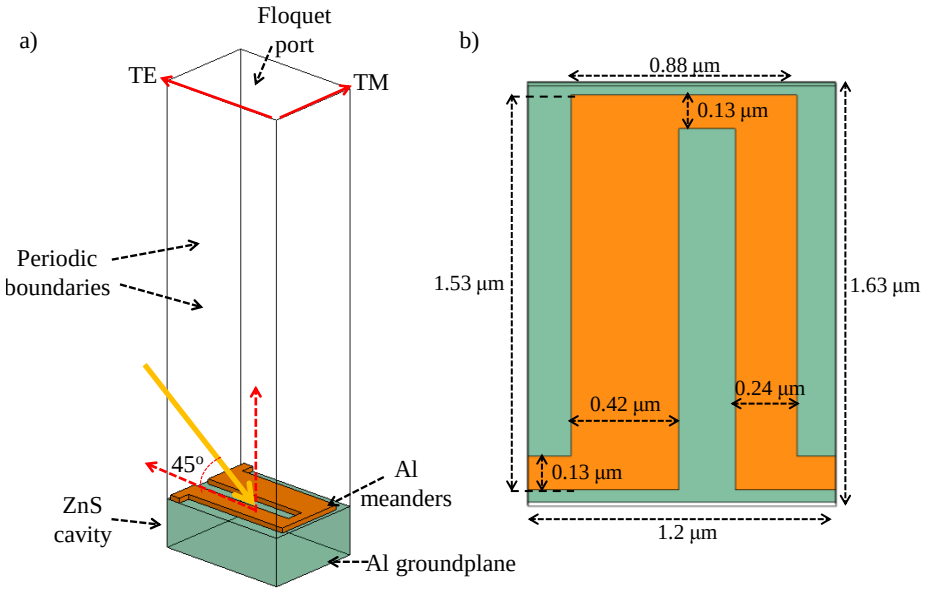

Fig. 3. Illustration of a) unit cell configuration in HFSS, where the yellow arrow represents the incident beam, and b) the optimized design parameters of the meanderline geometry.

The design was originally simulated with a 45° angle of incidence, in a plane parallel to the axis of periodicity associated with the equivalent TE mode of the meanderline grid (Fig. 2). The optical properties of each material used in the model were measured by spectroscopic

#146273 - $15.00 USD Received 19 Apr 2011; revised 6 May 2011; accepted 6 May 2011; published 13 May 2011

ellipsometry [23]. The meanderline elements and the groundplane were aluminum (Al), and the dielectric layer was zinc sulfide (ZnS), whose measured optical constants are shown in Fig. 4. Simulations were performed over the full LWIR band, and results from the optimized design are shown in Fig. 5.

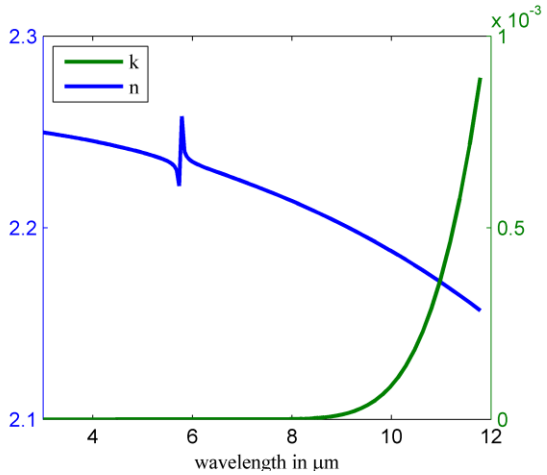

Fig. 4. Optical constants for ZnS measured by IR spectroscopic ellipsometry.

Specific parameters used for characterization of the reflective meanderline QWP are the phase retardance between the reflected TE and TM components, the axial ratio (AR), polarization-averaged power reflectivity, and the polarization conversion ratio (PCR). The AR is defined as the ratio between the two orthogonal E-field amplitudes [24]. In order to obtain perfect conversion from a 45° linearly-polarized (LP) incident field into CP output, a phase retardance of $\pi/2$ and an AR of 1 are desired. Figure 5 shows that the simulated phase retardance is very close to $\pi/2$ across the LWIR, and the AR < 2 over most of the band, which are good indicators of efficient conversion of LP into CP [17].

#146273 - $15.00 USD Received 19 Apr 2011; revised 6 May 2011; accepted 6 May 2011; published 13 May 2011

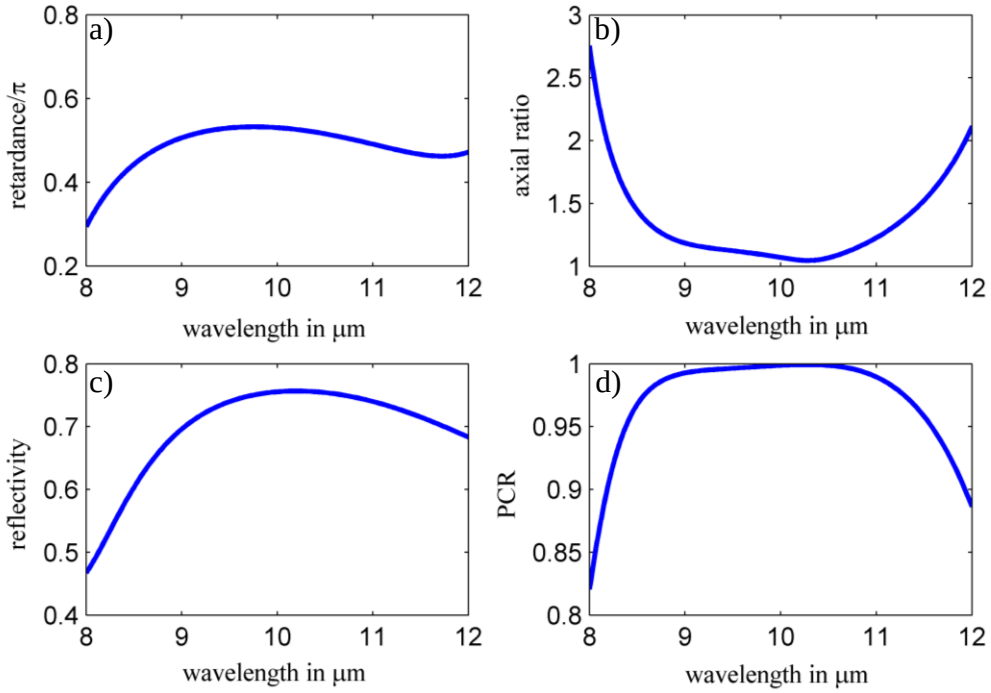

Fig. 5. Simulated polarimetric and power reflection parameters from HFSS, where a) is the spectral phase retardance, b) is the axial ratio, c) is the polarization-averaged power reflection coefficient, and d) is the polarization conversion ratio.

We also computed the percentage of circular polarization that is obtained upon reflection from the meanderline QWP. This polarization conversion ratio (PCR) can be written the ratio between the reflected state of polarization and the total field intensity [10]

$$PCR = \frac{\left(\sqrt{R_{TE}} - i \cdot \sqrt{R_{TM}} \cdot \exp(i \cdot \delta)\right)^2}{2 \cdot \left(R_{TE} + R_{TM}\right)}, \tag{1}$$

where R_{TE} and R_{TM} are the power-reflection coefficients for the TE and TM modes. Since the reflected orthogonal components are expected to be $\pi/2$ out of phase, the above formula results in a value of 1 when the TM component is phase-shifted by $\pi/2$ and the amplitudes are equal in magnitude, which signifies complete conversion of an incident 45° LP beam into CP. The simulated PCR plotted in Fig. 4 never dips below 85%, which suggests that the majority of the reflected beam will be CP. The power reflection coefficient, also shown in Fig. 5, was computed as the geometrical average between the reflected intensities of the TE and TM modes:

$$R_{total} = \frac{1}{2} \cdot \left(R_{TE} + R_{TM}\right). \tag{2}$$

The maximum reflected power is approximately 75%, which is adequate for some broadband imaging applications, although a higher efficiency would be required for use with high-powered laser systems. The materials that were selected for the design are representative of the best materials in the LWIR as far as ohmic loss and absorption are concerned. However, as Fig. 5 shows, there is still a significant power absorption caused by multiple reflections between the meanderline elements and the groundplane [25]. The tradeoff inherent in reflective meanderline QWPs, as compared to other design types, is that a lower power

#146273 - $15.00 USD Received 19 Apr 2011; revised 6 May 2011; accepted 6 May 2011; published 13 May 2011

efficiency is the cost for achieving broadband performance. The numerical results presented are representative of a structure optimized for power reflection that would give a broadband LP-to-CP conversion in reflection.

3. Fabrication and measurement of a reflective meanderline QWP

The submicron dimensions shown in Fig. 3 were fabricated by standard electron-beam (e-beam) lithography techniques [26]. Initially, a bare single-sided polished (SSP) silicon (Si) wafer was coated with an optically thick layer of Al, which served as the groundplane. Afterwards, a 650-nm layer of ZnS was deposited by thermal evaporation. Patterning of the subwavelength meanderline elements on top of the ZnS layer was carried out via e-beam lithography with a Leica EBPG 5000 + system. Once exposure and development of the array pattern was complete, evaporation of 60 nm of Al onto the exposed areas was performed with a multi-source high-vacuum AJA e-beam evaporation system. A precursor layer of chromium (Cr) 5 nm in thickness was evaporated beforehand to enhance adhesion of the Al onto the ZnS. After completion of the deposition process, the remaining metals and resists were lifted off in a sonic-agitation bath with N-dimethylacetamide solution as the resist remover. A final cleaning of the surface with organic solvents resulted in the structure shown in Fig. 6.

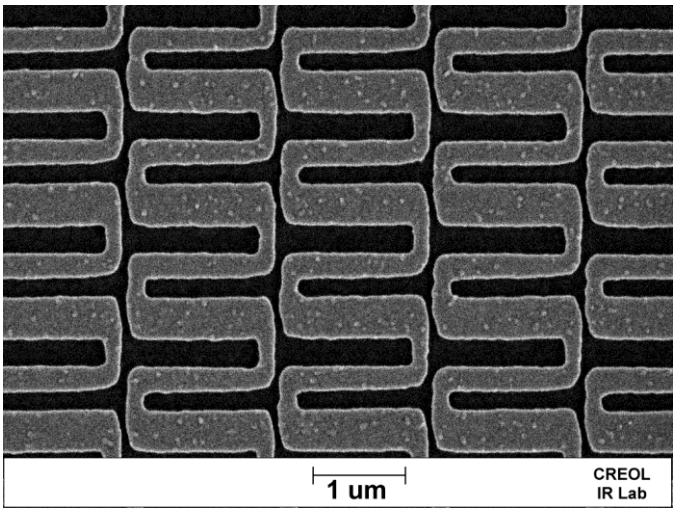

Fig. 6. SEM image of fabricated meanderline FSS array.

The completed structure was measured with an IR variable angle spectroscopic ellipsometer (IR-VASE) from J. A. Woollam, which measures the change in polarization upon reflection from a sample by extracting two polarimetric parameters; psi (ψ), the auxiliary angle of the reflected polarization ellipse, and delta (δ), the phase retardance between orthogonal components of the field [13,14,24]. It can measure the power reflection coefficient for both TE and TM polarizations, so this single instrument can acquire all the necessary spectral parameters that characterize the performance of the reflective meanderline QWP. The measurement coordinates of IR-VASE system are arranged such that TE and TM modes correspond to predefined directions on the sample holder. This is important, since the numerical optimizations of the meanderline design parameters defined the plane of incidence as being parallel to the grating periodicity of the meanderline array (Fig. 3). Thus, the periodicity axis of the meanderline QWP device is aligned with the TM coordinate axis of the IR-VASE system.

The polarization ellipse parameters ψ and δ were retrieved through a single spectroscopic scan at 45° angle of incidence on the IR-VASE instrument. The AR is given by the following equation [13,24]

#146273 - $15.00 USD Received 19 Apr 2011; revised 6 May 2011; accepted 6 May 2011; published 13 May 2011

$$AR = 1 \Big/ \left(\tan\left[\frac{1}{2} \arcsin\left\{ \sin(2 \cdot \psi) \cdot \sin(\delta) \right\} \right] \right). \quad (3)$$

With the power reflection constants of Eq. (2) acquired by a similar measurement process on the IR-VASE, all requisite data can be measured for comparison with the numerical FEM results.

4. Results and discussion

The measured spectrally-dependent phase retardance, AR, PCR, and power reflection coefficients are plotted on their respective graphs in Fig. 7.

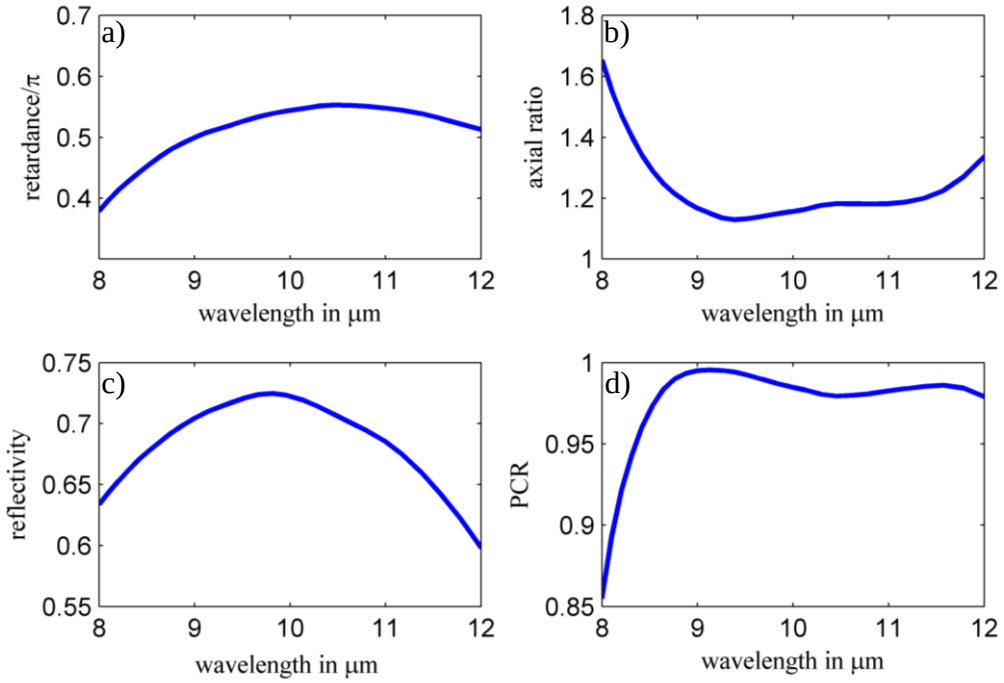

Fig. 7. Measured quantities from the IR-VASE, consisting of a) the phase retardance, b) axial ratio, c) average power reflection, and d) polarization conversion ratio.

Comparing the plots of Figs. 5 and 7, most of the differences between the model predictions and the experimental data can be attributed to slight differences between the modeled structure and the array elements that were actually fabricated. The SEM image of the meanderline array in Fig. 6 shows rounded edges of the element geometry instead of flat rectangular shapes, and the measured linewidths of the corresponding structure indicate that the pattern was slightly over exposed, resulting in enlarged linewidths than designed for by approximately 30%. The fabricated meanderline elements on Fig. 6 also exhibit some degree of surface roughness, which may have contributed to increased absorption losses and resistivity across the surface of the metal conductors. In addition, it was found that after evaporation, the thickness of the ZnS layer was about 580 nm rather than the design thickness of 650 nm. Regardless, the measured data seen in Fig. 7 demonstrates a reflective meanderline array above a groundplane that produces broadband CP upon reflection of a 45° LP field. The AR is below 2 over the entire LWIR band, and the phase retardance is quite achromatic near the desired $\pi/2$ value. Furthermore, the PCR is always above 85%, even at the edges of the band, showing a high-efficiency conversion of LP into CP. Finally, the polarization-averaged reflectivity has a maximum of approximately 72%, which is very close to the outcome of the

#146273 - $15.00 USD Received 19 Apr 2011; revised 6 May 2011; accepted 6 May 2011; published 13 May 2011

FEM model. The overall spectral dispersion in the experimental data agrees quite well with the values obtained from the FEM model.

In addition to the measurements that were performed at a 45° angle of incidence, the spectral phase retardance and AR were also measured over a 20° angular range centered on the 45°-incidence configuration (Fig. 8), to gauge the angular sensitivity of the device performance.

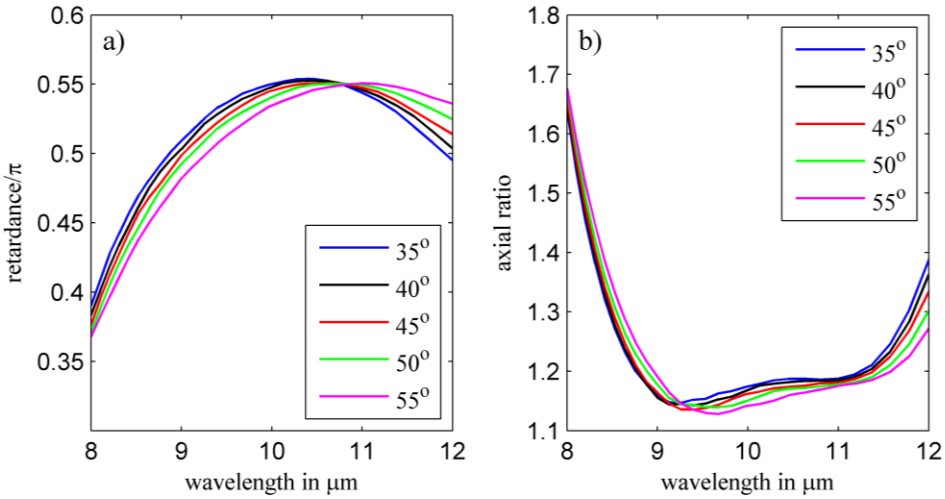

Fig. 8. Angular dependence of a) the phase retardance and b) the axial ratio over a 20° span around the optimum 45° angle of incidence.

The reflected state of polarization from the meanderline QWP is very stable with regard to incident angle. This is a beneficial characteristic that would allow the reflective meanderline technology to be incorporated in situations where the radiation is incident over a broad angular range. The device can thus be inserted into an optical system in non-collimated space, such as in the focusing beam of a polarization-resolved thermal imager.

5. Conclusion

We have presented results of simulations and measurements of a reflective meanderline QWP, which has significant spectral and angular bandwidths. Measurements were made over the 8-12 μm LWIR band, and over a 20° range of angles centered on 45°. The measured polarization conversion ratio was over 85% over the entire LWIR band. The polarization-averaged power reflectance exceeded 60% over the LWIR, and had a peak value of 72%. Good agreement was obtained between the computational-electromagnetic models and the measured data, which provides validation of the design approach for these types of devices in the infrared band. Future work may entail further refinement of the full-wave electromagnetic model to incorporate features that were observed after device fabrication, which would increase accuracy and account for manufacturing effects in the optimized design.

#146273 - $15.00 USD Received 19 Apr 2011; revised 6 May 2011; accepted 6 May 2011; published 13 May 2011